Improved adsorption of Congo red by nanostructured flower-like Fe(II)–Fe(III) hydroxy complex

Xiaoyan Sun, Zhongwu Liu, Zhigang Zheng, Hongya Yu and Dechang Zeng

ABSTRACT

Amorphous Fe(II)–Fe(III) hydroxy complex with flower-like nanostructure was synthesized by ferric reduction using a microwave-assisted ethylene glycol approach. Here we investigated the correlation between its chemical composition and the removal rate for Congo red (CR) dye. The results showed that the amorphous complex had similar reduction and anion exchange capacities to the green rust. Due to the synergistic effect of attractive electrostatic interaction, anion exchange, ferrous redox and hydrogen bonding, the Fe(II)–Fe(III) hydroxy complex exhibited strong adsorption of CR with an estimated adsorption capacity up to $513 \, \mathrm{mg \, g^{-1}}$. In contrast, the Fe(III) hydroxy complex had an adsorption capacity of $296 \, \mathrm{mg \, g^{-1}}$ because of the predominant mechanism based on the electrostatic interaction. The present study provides a facile synthesis of nanostructured iron hydroxy complex, with superior performance in adsorbing CR.

Key words | adsorption, Congo red, Fe(II)–Fe(III) hydroxy complex, flower-like structure, microwave-assisted synthesis

Xiaoyan Sun
Zhongwu Liu
Zhigang Zheng
Hongya Yu
Dechang Zeng (corresponding author)
School of Materials Science and Engineering,
South China University of Technology,
Guangzhou, 510640,
China
E-mail: medczeng@scut.edu.cn

INTRODUCTION

Owing to the huge damage of water pollution, increasing attention has been paid to water treatment in the past few decades. Azo dyes are extensively used in industrial coloring for plastics, fiber, paints, rubber and feathers. If industrial effluents with high azo dye contents were discharged into water bodies, it would cause ecological damage problems derived from their hazardous effects on living beings. Therefore, it is very meaningful to research the removal of organic azo dye from wastewater (Ahmad & Kumar 2010; Hao et al. 2014).

Iron-containing nanomaterials have received favor in water treatment due to their simplicity, high efficiency, and availability (Kharisov et al. 2012). Because of the charge redistribution ability (Wander et al. 2007) of reactive ferrous compounds and large surface area, the structural ferrous hydroxy complexes, such as green rusts (Hanna et al. 2010; Lu et al. 2016; Huang et al. 2017; Yin et al. 2017) and ferrous hydroxide complex (Shao et al. 2016; Roberts et al. 2017; Zhang et al. 2017), have higher reactivity in adsorption of heavy metals and removal of organic and inorganic pollutants. In most cases, the Fe_3O_4 (Cho et al. 2007; Jung et al. 2012) Fe_2O_3 (Wang et al. 2011; Fei et al. 2013) and γ-FeOOH

with good magnetic response were prepared by thermal treatment of the green or red precursor (Zhong et al. 2006). The precursor was usually described as iron alkoxide (Jung et al. 2012), $Fe(OH)_2$ or Fe(II)–Fe(III) hydroxide mixture. Although the calcined products can maintain original morphology, the surface properties and dispersion behavior in liquid phase will inevitably change. To the best of the authors' knowledge, there are few reports on the detailed analysis of the amorphous green precursor and its application in azo dye decolorization in aqueous solution. Hence, the rich ferrous precursor should be fully investigated.

Glycol method is a facile method to prepare ferrous-containing nanomaterials. It was reported that the reduction by ethylene glycol could maintain the iron ions in reduced Fe(II) form (Wiley et al. 2005). Herein, we prepared a type of nanostructured 3D flower-like Fe(II)–Fe(III) hydroxy complex by combining the glycol method (Cheng et al. 2011) and rapid microwave processing (Harpeness & Gedanken 2005; Zhang & Zhu 2008; Ai et al. 2010). Congo red (CR), an azo dye commonly used for staining in histology and microscopy, was selected as a model organic pollutant. The Fe(II)–Fe(III) hydroxy complex and its oxidized

products, Fe(III) hydroxide, were used to remove CR from aqueous. The effect of structural ferrous on the CR decolorization was investigated. Meanwhile, the underlying mechanism for the adsorption of CR by Fe(II)–Fe(III) hydroxy complex was analyzed in detail.

METHODS

Materials

Iron acetylacetonate (Fe(acac)$_3$, 98%) was purchased from Aladdin. Ethylene glycol (EG, 99%) was purchased from Sigma-Aldrich. All other chemicals were at least reagent grade and were used as received. All solutions were prepared in deionized water.

Synthesis of adsorbents

Fe(II)–Fe(III) hydroxy complex was synthesized through a polyolthermal procedure based on thermal decomposition of the precursors of Fe(acac)$_3$ in liquid polyol. For a typical synthesis, 0.354 g Fe(acac)$_3$ was added to 12.5 mL EG in a 60 mL Teflon reactor. With bubbled nitrogen, the mixture was stirred to give a wine-red solution. The reactor with the solution was placed in a microwave oven (WX-4000, Preekem, China) and the microwave reaction was heated to 180 °C with a heating rate of 10 °C min^{-1} and kept for 3 min. Solid green products were washed with absolute ethanol five times and separated by centrifugation. The green Fe(II)–Fe(III) hydroxy complex was dried in a vacuum at 60 °C overnight. The resulting green Fe(II)–Fe(III) hydroxy complex was re-dispersed in water without gas protection and stirred for 4 hours and 24 hours, respectively. Then, the red flocculation was centrifugally separated from the solution and dried in a vacuum at 60 °C overnight. The final 4 h- and 24 h-oxidized red products were generated.

Structure characterizations

All powder X-ray diffraction (XRD) measurements were performed with a Rigaku Ultima IV diffractometer using Cu-Kα radiation. The microstructure of as-synthesized samples was analyzed by scanning electron microscopy (SEM, NOVA NANOSEM 430) and transmission electron microscopy (TEM, JEOL-2100F). X-ray photoelectron spectroscopy (XPS) was carried on using an Axis Ultra DLD. The adsorption spectrum of the filtrate was measured on a Gold S54 UV-vis spectrophotometer. The zeta potential

of the selected sample was tested by a NANO-2S 90 (Malvern).

Adsorption of CR

The adsorption activities of the as-prepared nanostructures were evaluated by the adsorption of CR under dark conditions. The adsorbent (20 mg) with a concentration of 200 mg L^{-1} was introduced to 100 mg L^{-1} CR solution under stirring. At given stirring intervals, the reaction suspension was sampled and separated by centrifugation. The removal rate (%) was calculated by the following Equation (1),

$$\text{Removal rate (\%)} = \frac{100(C_0 - C_t)}{C_0} \tag{1}$$

where C_0 and C_t (mg L^{-1}) are the initial concentration of the CR solution and concentration at time t (min).

To estimate the adsorption capacity, 20 mg of the green Fe(II)–Fe(III) hydroxy complex and 24 h-oxidized red products were added to 100 mL of the CR solutions, varied in the range of 50–300 mg L^{-1}, and the solutions were stirred for 12 hours to reach the adsorption equilibrium. The equilibrium adsorption capacity (q_e) was calculated using Equation (2). Then the equilibrium adsorption data were fitted with Langmuir (Equation (3)) and Freundlich models (Equation (4)), respectively (Zhao *et al.* 2017)

$$q_e = (C_0 - C_e)V/m \tag{2}$$

$$q_e = \frac{q_m K_L C_e}{1 + K_L C_e} \tag{3}$$

$$q_e = K_F C_e^{1/n} \tag{4}$$

where C_e (mg L^{-1}) is the equilibrium concentration of the CR solution, q_m (mg g^{-1}) is the theoretical maximum adsorption capacity, V (L) is the volume of the solution, and m (g) is the mass of the adsorbent, K_L (L mg^{-1}) is the Langmuir constant related to the affinity of binding sites and K_F (mg g^{-1}) and n are the Freundlich constant relating to the adsorption intensity of the adsorbents, respectively.

For the recycling experiments, 20 mg of the adsorbents was added to 100 mL of the CR solution (100 mg L^{-1}). Each adsorption period was 4 hours. After each adsorption experiment, the adsorbent was collected and washed thoroughly with 0.5 mM NaOH solution and absolute ethanol several times and then dried in a vacuum at 60 °C overnight for reuse.

RESULTS AND DISCUSSION

Structure and morphology

A simple, rapid microwave-assisted polyol route was used for the synthesis of amorphous Fe(II)–Fe(III) hydroxy complex. The main advantages of the microwave-assisted synthesis are the accelerated reduction rate and the highly homogeneous size distribution of the produced nanoparticles. Figure 1 shows the SEM and TEM images of the green product obtained from microwave reactions. Flower-like architectures, denoted as Fe(II)–Fe(III) hydroxy complex, were observed with an average diameter of 1.5–3 μm. The TEM observations (Figure 1(c) and 1(d)) on a single structure reveal the building blocks of ultrathin nanosheets with smooth surfaces and the thickness less than 12 nm. Thus the green product is expected to exhibit a high specific surface area and a large adsorption capacity. With the help of microwave irradiation, the Fe(II)–Fe(III) hydroxy complex could nucleate quickly from the solvent, leading to plentiful nanocrystals aggregated and then assembled into the flower-like nanostructures, which can greatly reduce the interfacial energy of these small nanocrystals. In addition, it was found in the experiments that the morphology of the 3D hierarchical structure had no significant change after 24-hour oxidation in the deionized water.

The XRD patterns of the green and red products oxidized for 24 h are shown in Figure 2. Broad diffraction
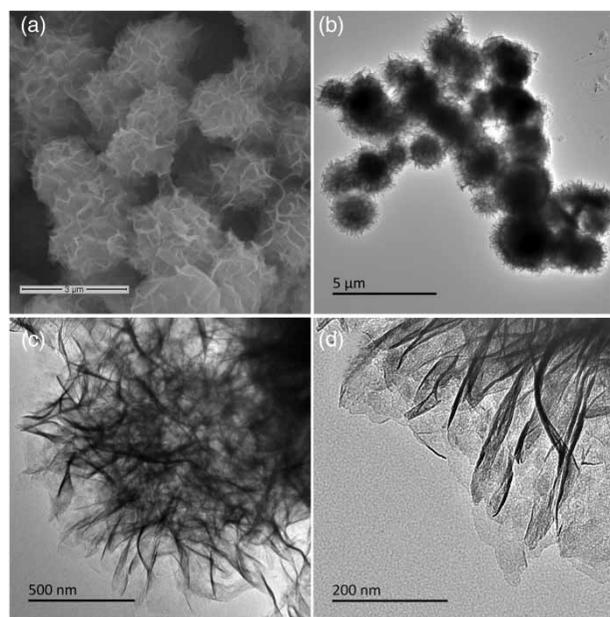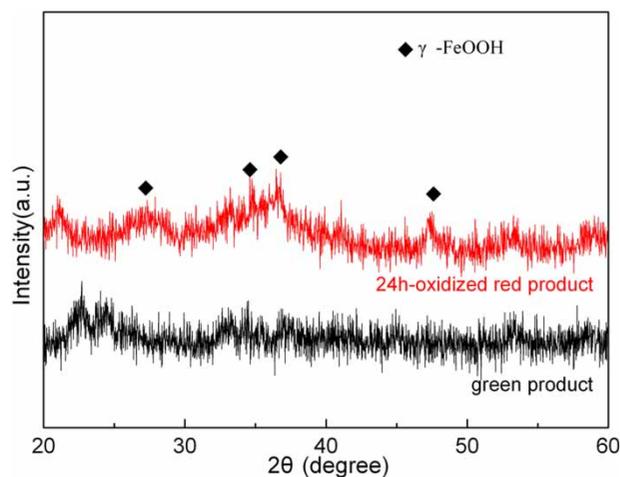

Figure 2 | XRD patterns of green Fe(II)–Fe(III) hydroxy complex and 24 h-oxidized product.

peaks of low intensity observed in the green product suggest the incomplete crystallization, while the reflections in the XRD pattern of the 24 h-oxidized sample could be assigned to γ-FeOOH (JCPDS file 08-0098).

Surface analysis of the green Fe(II)–Fe(III) hydroxy complex and 24 h-oxidized red products were carried out using XPS (Figure 3). The binding energy for the C 1s peak (284.6 eV) was used as an internal reference. Figure 3 (a) displays the fully scanned XPS spectra of the products, which indicates the existence of Fe, O and C elements. Figure 3(b) shows the XPS of Fe 2p spectra of the samples. The satellite peak at 719.7 eV highlights the difference between the green and the 24 h-oxidized red products. The photoelectron peaks at binding energies of 711.3 and 724.6 eV are the characteristic doublet of Fe 2p3/2 and 2p1/2 spectra for iron (hydro) oxide, respectively. The main peak at around 711.3 eV for the 24 h-oxidized red product is confirmed to be Fe^{3+} state as the distinct characteristic satellite peak at around 8.4 eV above the principal peak (Mclntyre & Zetaruk 1977; Han *et al.* 2011). The apparent lack of any satellite structure for the green product, in fact, results from a superposition of Fe^{2+} and Fe^{3+} associated satellite intensity at 715.7 and 719.7 eV. These results indicate that the green product contains both Fe^{2+} and Fe^{3+} on the surface. High-resolution XPS spectra of C1s were deconvoluted into three individual peaks: graphitic carbon (284.6 eV), C-OH (285.6–285.7 eV), and COOH (288.7 eV) (Zhao *et al.* 2017). After oxidation, the intensity of the peak at 285.6 eV decreased (Figure 3(c)). Figure 3(d) shows the O 1s spectra of the samples. After the samples were oxidized in water for 24 hours, the shoulder at 529.7 eV became an evident peak in the O ls band. According to previous reports (Seefeld *et al.* 2013), the peak at
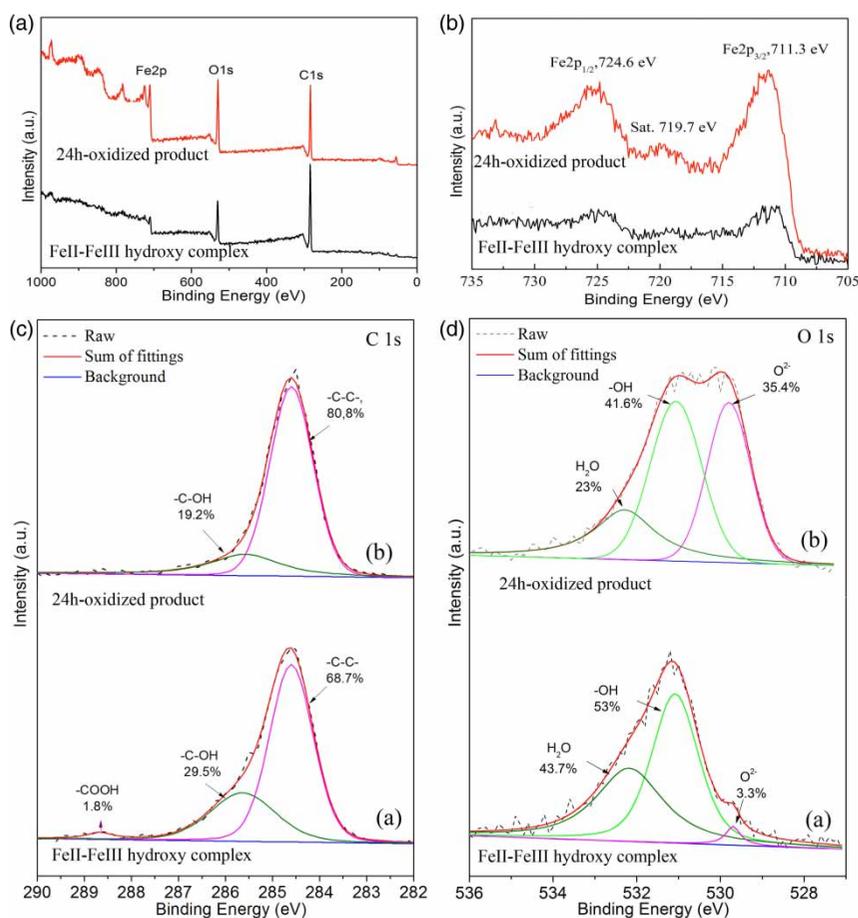

Figure 1 | (a) SEM and (b)–(d) TEM images of green Fe(II)–Fe(III) hydroxy complex.

Figure 3 | X-ray photoelectron spectroscopy spectra: (a) wide scan, (b) Fe 2p spectra, (c) C 1s and (d) O 1s spectra of Fe(II)–Fe(III) hydroxy complex and 24 h-oxidized product.

529.70 eV corresponds to a typical metal-oxygen bond, and the peak at 531.08 eV is usually associated with oxygen in -OH groups. The hydroxy may distribute inside and on the surface of the flower-like structure, and in agreement with the observation of FeOOH in XRD patterns. According to these results, the oxidization in water leads to a chemical change. Most of the divalent irons were oxidized to the trivalent state after exposure in water for 24 hours. Meanwhile, the content of hydroxy group decreased from 53% to 41.6% in view of the peaks at 531.08 eV. Based on the peaks fitting in C 1s and O 1s spectra, the reduced hydroxy species should be mainly alcoholic hydroxyl group (C-OH). Coexistence of Fe(II) and Fe(III) in such an amorphous iron species could possibly represent the green rust with interca-lated alcoholic anions.

CR adsorption

The adsorption activities of Fe(II)–Fe(III) hydroxy complex and 4 h-oxidized product were demonstrated using CR. It is observed that the absorption spectrum (Figure 4) of CR in water is characterized by one maximum band in the visible region located at 500 nm and by two bands in the ultraviolet region located at 238 and 340 nm. The maximum at 500 nm results from the conjugate system of -N=N- and naphthalene ring (Florenza et al. 2014). The absorbance peaks at 238 and 340 nm are due to the benzene and naphthalene rings, respectively (Wu et al. 2000; Stylidi et al. 2003). When the Fe(II)–Fe(III) hydroxy complex was used as the sorbents, the absorbency of naphthalene and azo group at 340 and 500 nm decreased faster than that of the benzene ring at 238 nm, suggestive of free aromatic aniline generated during the surface adsorption. This may result from the sur-face reduction of structural ferrous. The ferrous, which leads to the rapidly increased adsorption capacity, was oxi-dized to ferric by the deionized water. Figure 5 shows the adsorption rate curves of CR using Fe(II)–Fe(III) hydroxy complex and the products oxidized for 4 h and 24 h, respec-tively. According to Figure 5, the equilibrium time for the adsorption of CR by Fe(II)–Fe(III) mixture decreases with
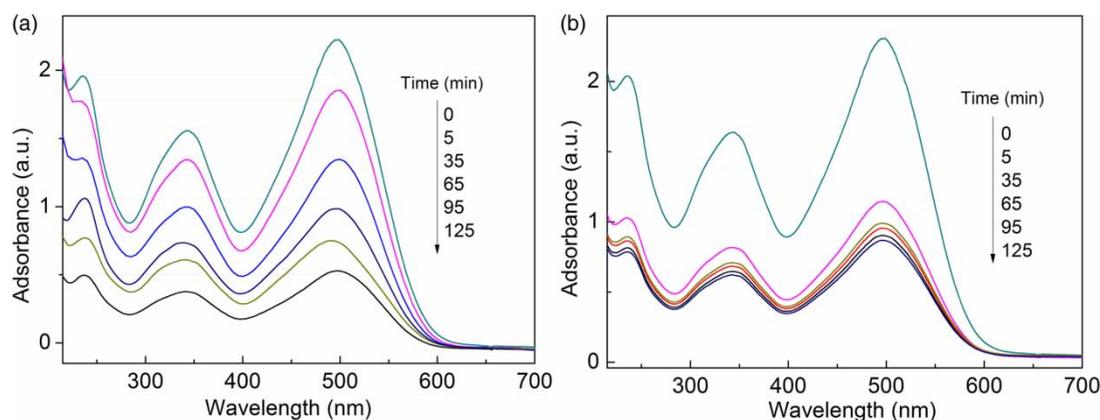
Figure 4 | UV-vis absorption spectra of CR solutions treated by as-prepared (a) Fe(II)–Fe(III) hydroxy complex and (b) 24 h-oxidized product. Experimental conditions: [CR] = 100 mg L^{-1}, V = 100 mL, adsorbent = 20 mg, pH = 6.8 (natural), T = 298 K.

the increased oxidation time in the range of 120–500 min. The increased equilibrium time indicates that CR on green Fe(II)–Fe(III) mixture is adsorbed by chemical activation or chemisorption. The removal rate of CR by the green Fe(II)–Fe(III) hydroxy complex in 4 hours is 91%, almost twice as much as that by red oxidized Fe(III) hydroxide (50%).

To understand the relationship between the adsorbent and the adsorbate at equilibrium and to estimate the maximum adsorption capacity of Fe(II)–Fe(III) hydroxy complex and 24 h-oxidized product, the effect of the CR concentration on adsorption was analyzed. The Freundlich model fails to produce a satisfied fit on the experimental data, whereas the Langmuir equation shows a very good agreement with experimental data, as indicated by the correlation coefficient $R^2 > 0.99$ (Figure 6). Therefore, CR sorption should occur through a monolayer adsorption on the

heterogeneous surface of adsorbents. Calculated maximum sorption capacities were 513 mg g^{-1} and 296 mg g^{-1} for Fe(II)–Fe(III) hydroxy complex and 24 h-oxidized products, respectively. These values are higher than those of many previously reported adsorbents under optimum conditions, such as hollow nestlike α-Fe$_2$O$_3$ nanostructures (Wei *et al.* 2013), and nanocrystalline Fe$_3$O$_4$ xerogel (Gao *et al.* 2016), suggestive of the potential applications of these hierarchically assembled 3D nanostructures in water treatment.

Zeta potentials and Fourier transform infrared (FTIR) tests were also employed to inspect the adsorption mechanism. Zeta potentials (as shown in Figure 7) of the green Fe(II)–Fe(III) hydroxy complex and the 24 h-oxidized red product were +31.3 and +20.4 mV, respectively. The positively charged surface is generally induced by the protonation of the surface hydroxyl groups. The decrease of zeta
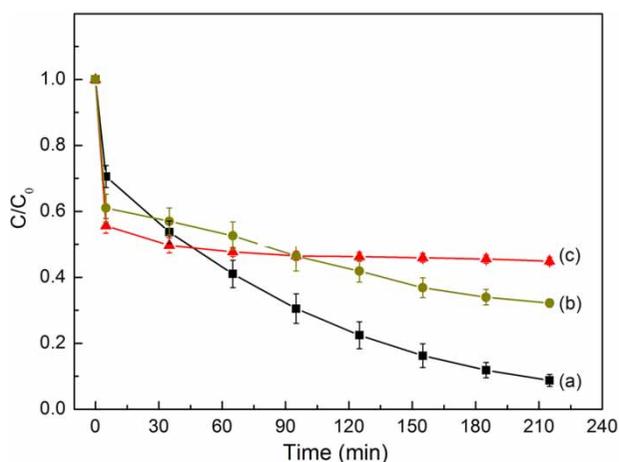

Figure 5 | The adsorption rate curves of CR at 500 nm using three different adsorbents: (a) Fe(II)–Fe(III) hydroxy complex, (b) 4 h-oxidized product and (c) 24 h-oxidized product.
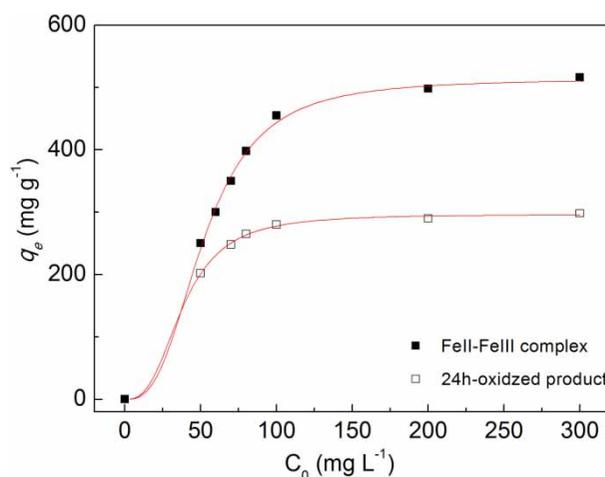

Figure 6 | Effect of initial concentration of CR on its adsorption on the Fe(II)–Fe(III) hydroxy complex (solid squares) and 24 h-oxidized product (hollow squares). Lines indicate the result of modeling using the Langmuir equation.
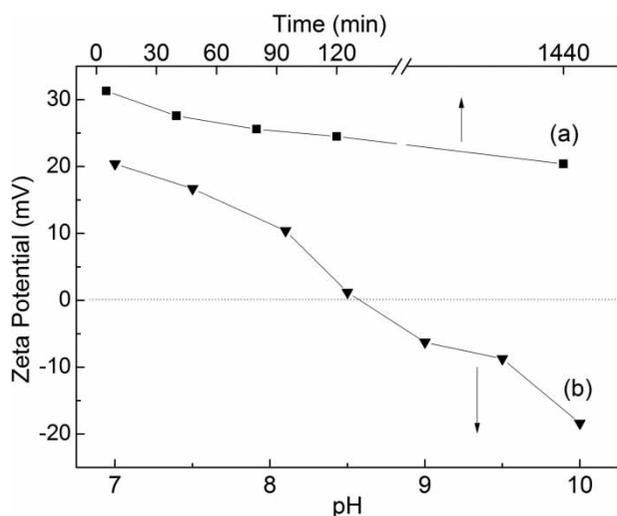
Figure 7 | Zeta potential variations (a) with time for the green Fe(II)–Fe(III) hydroxy complex and (b) with pH value for the 24 h-oxidized product.

potentials results from the decreased content of the alcoholic hydroxyl analyzed by XPS. Zeta potential measurements show that the overall red rust surface is positively charged and the anionic group $-SO_3^-$ of CR may develop attractive electrostatic interactions with $Fe-OH_2^+$. The accentuated adsorption of CR in aqueous solutions in the beginning suggests that the electrostatic factors control the adsorption process (Bao *et al.* 2013). Although the Fe(II)–Fe(III) hydroxy complex is more positively charged than its oxidized products, the decolorization rate in the beginning (ca. 5 minutes) is increased with oxidization time. The anomaly indicates more than one adsorption mechanism existed in the process. We propose anion exchange between Fe(II)–Fe(III) hydroxy complex and CR. From the adsorption behavior, the adsorption mechanism should be a synergistic effect of the surface reduction (Kong *et al.* 2014), hydrogen bonding (Ai *et al.* 2010; Liu *et al.* 2014), anion exchange and electrostatic interactions. The underlying mechanism will be discussed later in detail.

Recyclability is also one of the most important issues for the practical applications of adsorbents. Herein, we found that, with inactive surface, the Fe(III) hydroxide complex can be easily separated by natural sedimentation. Zeta potential determination shows that pH value of zero charge (pH_z) for the 24 h-oxidized product is 8.5. Above pH_Z, the whole surface of adsorbents is negatively charged and electrostatic interaction between CR and adsorbents' surface disappears. Addition of NaOH is a simple and effective way for desorption. The main mechanism of desorption is the inversion of surface charge to weak attractive electrostatic. Meanwhile the OH^- ions can displace organic anion

species in adsorbent. Figure 8 shows the statistical removal rate of CR (100 mL, 100 mg L^{-1}) by the green Fe(II)–Fe(III) hydroxy complex (20 mg) after successive recycle numbers. The total removal amount of CR decreases with recycle number. To emphasize the change of adsorbents, the removal amount was divided into two parts, fast removal in the beginning (ca. 5 minutes) and slow removal after 5 minutes. The statistical figure shows that the second-step removal amount decreases gradually instead of disappearing directly. The coexistence of ferrous and alcoholic hydroxyl species can increase the maximum adsorption capacity and slow the adsorption rate of CR dye. This increase may result from three effects related to Fe(II)–Fe(III) reactivity, i.e., the reduction of -N=N- group to amine and the complexation with CR or by-product by $Fe-OH\cdots NC_6H_5$ hydrogen bonding (Wang & Wang 2008). Meanwhile, the oxidation of ferrous to ferric leads to the formation of hydroxyl groups, which also slows down the adsorption rate.

Figure 9 presents the FTIR spectra of 24 h-oxidized products before adsorption, after adsorption and after desorption of CR. The bands at 1,019, 743 and 553 cm^{-1} are characteristic peaks of γ-FeOOH. Two absorption bands at ~3,440 and ~1,640 cm^{-1} are attributed to the physically adsorbed H_2O molecules (Lei *et al.* 2018). After CR adsorption, the observed wide peak at 3,440 cm^{-1} resulted from overlapped stretching vibration of N-H on CR (Ahmad & Kumar 2010). Meanwhile, the peak at 1,640 cm^{-1} undertakes a reversible shift to 1,628 cm^{-1} after adsorption, suggestive of the hydrogen bond involved in the adsorption process (Wang & Wang 2008). The bands in the 1,225–1,044 cm^{-1} regions, owing to S=O stretching, also disappear after desorption. Furthermore,
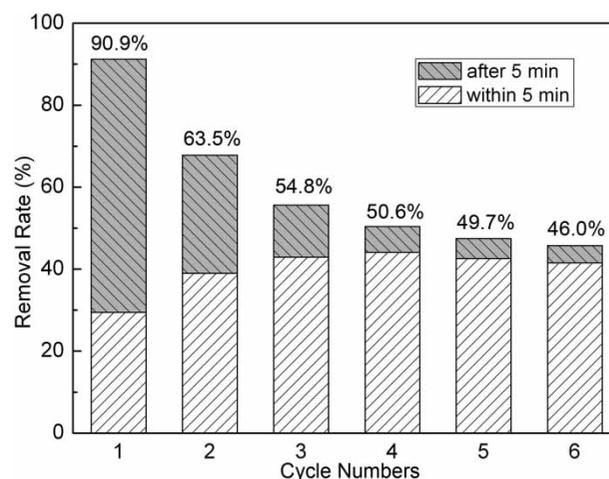

Figure 8 | The final removal rate of CR treated by the as-prepared Fe(II)–Fe(III) hydroxy complex (20 mg) versus cycle numbers.
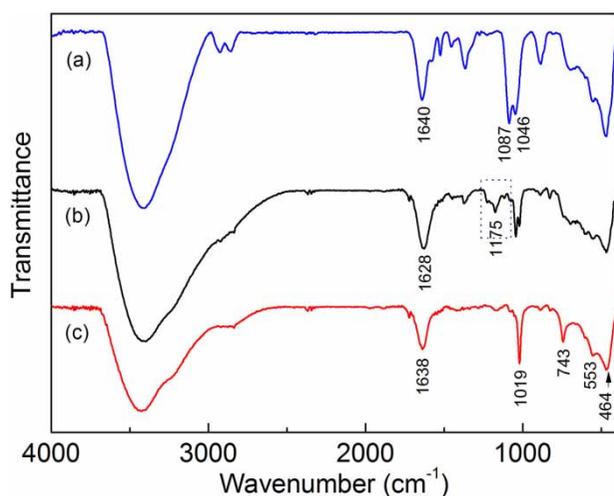
Figure 9 | FTIR spectra of 24 h-oxidized products (a) before CR adsorption, (b) after adsorption of CR and (c) after desorption of CR by adding NaOH.

the peaks at 1,087 and 1,046 cm^{-1} assigned to EG diminish after adsorption and disappear after the complete desorption using NaOH solution. This indicates that the metastable alcohol ligand is sensitive to anion. Attacked by OH^{-}, the Fe(II)–Fe(III) hydroxy complex can be converted to FeOOH by losing organic anion species. These results implied that the adsorption of CR onto Fe(II)–Fe(III) hydroxy complex was governed by chemical activation or chemisorptions (Wang & Wang 2008; Lei *et al.* 2018).

The results indicate that the constituents of ferrous and alcohol hydroxy species determine the adsorption rate. From the view of adsorption ability, ferrous and alcohol hydroxy species favor the electrostatic attraction, which is mainly responsible for the decolorization in the beginning (ca. 5 minutes). It is also noted that electrostatic adsorption takes priority over anion exchange and hydrogen bonding in the case of excess adsorbent. The enhanced decolorization of CR by Fe(II)–Fe(III) hydroxy complex should be more durable under anoxic conditions and the structural Fe(III) may be reduced to Fe(II) by hydroxylamine reduction (Han *et al.* 2014) or electrochemical reduction (Soltermann *et al.* 2014), which is under investigation. The excellent ferrous redox, anion exchange and electrostatic attraction of Fe(II)–Fe(III) hydroxy complex found in the present work would endow the possibility of their practical applications.

CONCLUSIONS

In this work, the flower-like Fe(II)–Fe(III) hydroxy complex was prepared by a low temperature glycol process with microwave assistance. The flower-like Fe(II)–Fe(III) hydroxy complex can be oxidized *in situ* to Fe(III) hydroxy complex in aqueous solution. The self-assembled flower-like structure is stable and suitable for solid–liquid separation. The Fe(II)–Fe(III) hydroxy complex has a high maximum adsorption capacity of 513 mg g^{-1}, while the adsorption capacity of the Fe(III) hydroxy complex is 296 mg g^{-1}. Oxygen-containing functional groups on Fe(II)–Fe(III) hydroxy complex play an important role for the CR adsorption. The superior adsorption performance of flower-like Fe(II)–Fe(III) hydroxy complex results from the synergistic action of attractive electrostatic, anion exchange, ferrous redox and hydrogen bonding. The enhanced decolorization of CR can be obtained by the Fe(II)–Fe(III) hydroxy complex until it is gradually converted to stable Fe(III) hydroxide. In addition, the flower-like Fe(II)–Fe(III) hydroxy complex is also expected to show high reactivity in pollutant reduction and as a potential Fenton catalyst.

REFERENCES

Ahmad, R. & Kumar, R. 2010 Adsorptive removal of Congo red dye from aqueous solution using bael shell carbon. *Applied Surface Science* **257**, 1628–1633.

Ai, Z. H., Deng, K. J., Wan, Q. F., Zhang, L. Z. & Lee, S. C. 2010 Facile microwave-assisted synthesis and magnetic and gas sensing properties of Fe$_3$O$_4$ nanoroses. *Journal of Physical Chemistry C* **114**, 6237–6242.

Bao, N., Li, Y., Yu, X. H., Niu, J. J., Wu, G. L. & Xu, X. H. 2013 Removal of anionic azo dye from aqueous solution via an adsorption-photosensitized regeneration process on a TiO$_2$ surface. *Environmental Science and Pollution Research* **20**, 897–906.

Cheng, C. M., Xu, F. J. & Gu, H. C. 2011 Facile synthesis and morphology evolution of magnetic iron oxide nanoparticles in different polyol processes. *New Journal of Chemistry* **35**, 1072–1079.

Cho, S. B., Noh, J. S., Park, S. J., Lim, D. Y. & Choi, S. H. 2007 Morphological control of Fe$_3$O$_4$ particles via glycothermal process. *Journal of Materials Science* **42**, 4877–4886.

Fei, J. B., Zhao, J., Du, C. L., Ma, H. C., Zhang, H. & Li, J. B. 2013 The facile 3D self-assembly of porous iron hydroxide and oxide hierarchical nanostructures for removing dyes from wastewater. *Journal of Materials Chemistry A* **1**, 10300–10305.

Florenzaa, X., Solano, A. M. S., Centellas, F., Martínez-Huitle, C. A., Brillas, E. & Garcia-Segura, S. 2014 Degradation of the azo dye Acid Red 1 by anodic oxidation and indirect electrochemical processes based on Fenton's reaction chemistry. Relationship between decolorization, mineralization and products. *Electrochimica Acta* **142**, 276–288.

Gao, J., Wei, W., Shi, M., Han, H., Lu, J. & Xie, J. 2016 A controlled solvethermal approach to synthesize nanocrystalline iron oxide for Congo red adsorptive removal from aqueous solutions. *Journal of Materials Science* **51**, 4481–4494.

Han, Y. S., Jeong, H. Y., Demond, A. H. & Hayes, K. F. 2011 X-ray absorption and photoelectron spectroscopic study of the association of As(III) with nanoparticulate FeS and FeS-coated sand. *Water Research* **45**, 5727–5735.

Han, D. H., Wan, J. Q., Ma, Y. W., Wang, Y., Huang, M. Z., Chen, Y. M., Li, D. Y., Guan, Z. Y. & Li, Y. 2014 Enhanced decolorization of Orange G in a Fe(II)-EDDS activated persulfate process by accelerating the regeneration of ferrous iron with hydroxylamine. *Chemical Engineering Journal* **256**, 316–323.

Hanna, K., Kone, T. & Ruby, C. 2010 Fenton-like oxidation and mineralization of phenol using synthetic Fe(II)-Fe(III) green rusts. *Environmental Science and Pollution Research* **17**, 124–134.

Hao, T., Yang, C., Rao, X. H., Wang, J. D., Niu, C. G. & Su, X. T. 2014 Facile additive-free synthesis of iron oxide nanoparticles for efficient adsorptive removal of Congo red and Cr(VI). *Applied Surface Science* **292**, 174–180.

Harpeness, R. & Gedanken, A. 2005 The microwave-assisted polyol synthesis of nanosized hard magnetic material, FePt. *Journal of Materials Chemistry* **15**, 698–702.

Huang, L. Z., Hansen, H. C. B. & Daasbjerg, K. 2017 Graphene oxide-mediated rapid dechlorination of carbon tetrachloride by green rust. *Journal of Hazardous Materials* **323**, 690–697.

Jung, Y., Son, Y. H. & Lee, J. K. 2012 3-D self-assembly of flower-like particles via microwave irradiation for water treatment. *RSC Advances* **2**, 5877–5884.

Kharisov, B. I., Rasika, Dias H. V., Kharissova, O. V., Jiménez-Pérez, V. M., Pérez, B. O. & Flores, B. M. 2012 Iron-containing nanomaterials: synthesis, properties, and environmental applications. *RSC Advances* **2**, 9325–9358.

Kong, F. Y., Wang, A. J., Cheng, H. Y. & Liang, B. 2014 Accelerated decolorization of azo dye Congo red in a combined bioanode-biocathode bioelectrochemical system with modified electrodes deployment. *Bioresource Technology* **151**, 332–339.

Lei, C. S., Pi, M., Cheng, B., Jiang, C. J. & Qin, J. Q. 2018 Fabrication of hierarchical porous ZnO/NiO hollow microspheres for adsorptive removal of Congo red. *Applied Surface Science* **435**, 1002–1010.

Liu, S. G., Ding, Y. Q., Li, P. F., Diao, K. S., Tan, X. C., Lei, F. H., Zhan, Y. H., Li, Q. M., Huang, B. & Huang, Z. Y. 2014 Adsorption of the anionic dye Congo red from aqueous solution onto natural zeolites modified with N,N-dimethyl dehydroabietylamine oxide. *Chemical Engineering Journal* **248**, 135–144.

Lu, Y. S., Yang, X. X., Wu, Z. L., Xu, L. & Xu, Y. F. 2016 A novel control strategy for N_2O formation by adjusting E_h in nitrite/Fe(II–III) carbonate green rust system. *Chemical Engineering Journal* **304**, 579–586.

McIntyre, N. S. & Zetaruk, D. G. 1977 X-ray photoelectron spectroscopic studies of iron oxides. *Analytical Chemistry* **49**, 1521–1529.

Roberts, H. E., Morris, K., Law, G. T. W., Mosselmans, J. F. W., Bots, P., Kvashnina, K. & Shaw, S. 2017 Uranium(V) incorporation mechanisms and stability in Fe(II)/Fe(III) (oxyhydr)oxides. *Environmental Science & Technology Letter* **4**, 421–426.

Seefeld, S., Limpinsel, M., Liu, Y., Farhi, N., Weber, A., Zhang, Y. N., Berry, N., Kwon, Y. J., Perkins, C. L., Hemminger, J. C., Wu, R. Q. & Law, M. 2013 Iron pyrite thin films synthesized from an Fe(acac)$_3$ ink. *Journal of the American Chemical Society* **135**, 4412–4424.

Shao, B. B., Guan, Y. Y., Tian, Z. Y., Guan, X. H. & Wu, D. L. 2016 Advantages of aeration in arsenic removal and arsenite oxidation by structural Fe(II) hydroxides in aqueous solution. *Colloids and Surfaces A: Physicochemical and Engineering Aspects* **506**, 703–710.

Soltermann, D., Baeyens, B., Bradbury, M. H. & Fernandes, M. M. 2014 Surface complexation modeling. *Environmental Science & Technology* **48**, 8698–8705.

Stylidi, M., Kondarides, D. I. & Verykios, X. E. 2003 Pathways of solar light-induced photocatalytic degradation of azo dyes in aqueous TiO$_2$ suspensions. *Applied Catalysis B: Environmental* **40**, 271–286.

Wander, M. C. F., Rosso, K. M. & Schoonen, M. A. A. 2007 Structure and charge hopping dynamics in green rust. *Journal of Physical Chemistry C* **111**, 11414–11423.

Wang, L. & Wang, A. Q. 2008 Adsorption properties of Congo red from aqueous solution onto surfactant-modified montmorillonite. *Journal of Hazardous Materials* **160**, 173–180.

Wang, L. L., Fei, T., Lou, Z. & Zhang, T. 2011 three-dimensional hierarchical flowerlike α-Fe$_2$O$_3$ nanostructures: synthesis and ethanol-sensing properties. *ACS Applied Materials & Interface* **3**, 4689–4694.

Wei, Z., Xing, R., Zhang, X., Liu, S., Yu, H. & Li, P. 2013 Facile template-free fabrication of hollow nestlike α-Fe$_2$O$_3$ nanostructures for water treatment. *ACS Applied Materials & Interface* **5**, 598–604.

Wiley, B., Sun, Y. G. & Xia, Y. N. 2005 Polyol synthesis of silver nanostructures: control of product morphology with Fe(II) or Fe(III) species. *Langmuir* **21**, 8077–8080.

Wu, F., Deng, N. S. & Hua, H. L. 2000 Degradation mechanism of azo dye C. I. reactive red 2 by iron powder reduction and photooxidation in aqueous solutions. *Chemosphere* **41**, 1233–1238.

Yin, W. Z., Huang, L. Z., Pedersen, E. B., Frandsen, C. & Hansen, H. C. B. 2017 Glycine buffered synthesis of layered iron(II)-iron(III) hydroxides (green rusts). *Journal of Colloid and Interface Science* **497**, 429–438.

Zhang, L. & Zhu, Y. J. 2008 Microwave-assisted solvothermal synthesis of AlOOH hierarchically nanostructured microspheres and their transformation to γ-Al$_2$O$_3$ with similar morphologies. *Journal of Physical Chemistry C* **112**, 16764–16768.

Zhang, C., Li, Y. Z., Wang, T. J., Jiang, Y. P. & Fok, J. 2017 Synthesis and properties of a high-capacity iron oxide adsorbent for fluoride removal from drinking water. *Applied Surface Science* **425**, 272–281.

Zhao, J. Q., Lu, Z. X., He, X., Zhang, X. F., Li, Q. Y., Xia, T. & Zhang, W. 2017 Fabrication and characterization of highly porous Fe(OH)$_3$@cellulose hybrid fibers for effective removal of Congo red from contaminated water. *ACS Sustainable Chemistry & Engineering* **5**, 7723–7732.

Zhong, L. S., Hu, J. S., Liang, H. P., Cao, A. M., Song, W. G. & Wan, L. J. 2006 Self-assembled 3D flowerlike iron oxide nanostructures and their application in water treatment. *Advanced Materials* **18**, 2426–2431.